Research Article | Vol. 8, No. 3 | 1 Mar 2018 | OPTICAL MATERIALS EXPRESS 522
Optical Materials EXPRESS

Spectral-luminescent properties of vapor deposited Cr:ZnS thin films and their application as saturable absorbers for 1.5-μm erbium lasers

Nikolai Tolstik,[1,2,*] Evgeni Sorokin,[3] Eric A. Karhu,[1] Konstantin Gorbachenya,[4] Stanislav M. Polyakov,[1] Viktor E. Kisel,[4] Nikolai Kuleshov,[4] Vedran Furtula,[1] Ursula J. Gibson,[1,5] and Irina T. Sorokina[1]

[1]*Department of Physics, NTNU - Norwegian University of Science and Technology, N-7491 Trondheim, Norway*
[2]*ATLA Lasers AS, Richard Birkelands vei 2B, N-7491 Trondheim, Norway*
[3]*Institut für Photonik, TU Wien, Gusshausstrasse 27/387, A-1040 Vienna, Austria*
[4]*Center for Optical Materials and Technologies, Belarusian National Technical University, 220013 Minsk, Belarus*
[5]*Department of Applied Physics, KTH Royal Institute of Technology, Stockholm, Sweden*
**nikolai.tolstik@ntnu.no*

Abstract: We report the results of the extensive spectral-luminescent characterization including concentration quenching analysis of the first laser-quality vapor-deposited Cr:ZnS films, and demonstrate their use as saturable absorbers. Comparison of spectral-luminescent properties with bulk Cr:ZnS indicates their high laser quality, opening the way towards industrial mid-IR thin-disk and waveguide lasers. Successful implementation of the grown films in a Q-switched Er,Yb:GdAB solid-state laser emitting at 1.52 μm gives clear experimental evidence of the high quality of the films.

OCIS codes: (310.6860) Thin films, optical properties; (160.6990) Transition-metal-doped materials; (300.6280) Spectroscopy, fluorescence and luminescence.

References and links

1. L. D. DeLoach, R. H. Page, G. D. Wilke, S. A. Payne, and W. P. Krupke, "Transition metal-doped zinc chalcogenides: spectroscopy and laser demonstration of a new class of gain media," IEEE J. Quantum Electron. **32**(6), 885–895 (1996).
2. I. T. Sorokina, "Cr^{2+}-doped II–VI materials for lasers and nonlinear optics," Opt. Mater. **26**(4), 395–412 (2004).
3. I. Sorokina and E. Sorokin, "Femtosecond Cr^{2+}-Based Lasers," IEEE J. Sel. Top. Quantum Electron. **21**(1), 1601519 (2015).
4. A. Sennaroglu, A. Ozgun Konza, and C. R. Pollock, "Continuous-wave power performance of a 2.47-μm Cr^{2+}:ZnSe laser: experiment and modeling," IEEE J. Quantum Electron. **36**(10), 1199–1205 (2000).
5. K. L. Schepler, R. D. Peterson, P. A. Berry, and J. B. McKay, "Thermal effects in Cr^{2+}:ZnSe thin disk lasers," IEEE J. Sel. Top. Quantum Electron. **11**(3), 713–720 (2005).
6. S. B. Mirov, V. V. Fedorov, D. Martyshkin, I. S. Moskalev, M. Mirov, and S. Vasilyev, "Progress in mid-IR lasers based on Cr and Fe-doped II-VI chalcogenides," IEEE J. Sel. Top. Quantum Electron. **21**(1), 1601719 (2015).
7. J. R. Macdonald, S. J. Beecher, A. Lancaster, P. A. Berry, K. L. Schepler, S. B. Mirov, and A. K. Kar, "Compact Cr:ZnS channel waveguide laser operating at 2,333 nm," Opt. Express **22**(6), 7052–7057 (2014).
8. I. T. Sorokina, V. Dvoyrin, N. Tolstik, and E. Sorokin, "Mid-IR ultrashort pulsed fiber-based lasers," IEEE J. Sel. Top. Quantum Electron. **20**(5), 0903412 (2014).
9. S. Xie, N. Tolstik, J. C. Travers, E. Sorokin, C. Caillaud, J. Troles, P. S. J. Russell, and I. T. Sorokina, "Coherent octave-spanning mid-infrared supercontinuum generated in As2S3-silica double-nanospike waveguide pumped by femtosecond Cr:ZnS laser," Opt. Express **24**(11), 12406–12413 (2016).
10. I. T. Sorokina, E. Sorokin, S. Mirov, V. Fedorov, V. Badikov, V. Panyutin, and K. I. Schaffers, "Broadly tunable compact continuous-wave Cr^{2+}:ZnS laser," Opt. Lett. **27**(12), 1040–1042 (2002).

#313192 https://doi.org/10.1364/OME.8.000522
Journal © 2018 Received 9 Nov 2017; revised 5 Jan 2018; accepted 9 Jan 2018; published 6 Feb 2018

Optical Materials EXPRESS

11. V. Philippov, A. Abdolvand, J. Nilsson, W. A. Clarkson, V. E. Kisel, V. G. Shcherbitsky, N. V. Kuleshov, V. I. Konstantinov, and V. I. Levchenko, "Passively Q-switched Er-Yb double clad fiber laser with Cr^{2+}:ZnSe and Co^{2+}:$MgAl_2O_4$ as a saturable absorber," Proc. SPIE **5335**, 8–15 (2004).
12. V. E. Kisel, V. G. Shcherbitsky, N. V. Kuleshov, L. I. Postnova, V. I. Levchenko, B. I. Galagan, B. I. Denker, and S. E. Sverchkov, "Passive Q switches for a diode-pumped erbium glass laser," Quantum Electron. **35**(7), 611–614 (2005).
13. K. N. Gorbachenya, V. E. Kisel, A. S. Yasukevich, M. B. Prudnikova, V. V. Maltsev, N. I. Leonyuk, S. Y. Choi, F. Rotermund, and N. V. Kuleshov, "Passively Q-switched Er,Yb:$GdAl_3(BO_3)_4$ laser with single-walled carbon nanotube based saturable absorber," Laser Phys. Lett. **14**(3), 035802 (2017).
14. K. Gorbachenya, V. Kisel, A. Yasukevich, P. Loiko, X. Mateos, V. Maltsev, N. Leonyuk, M. Aguiló, F. Díaz, U. Griebner, V. Petrov, and N. Kuleshov, "Graphene Q-switched Er,Yb:$GdAl_3(BO_3)_4$ laser at 1550 nm," Appl. Opt. **56**(16), 4745–4749 (2017).
15. D. Zhou, L. Wei, B. Dong, and W. Liu, "Tunable passively Q-switched erbium-doped fiber laser with carbon nanotubes as a saturable absorber," IEEE Photonics Technol. Lett. **22**(1), 9–11 (2010).
16. L. Liu, Z. Zheng, X. Zhao, S. Sun, Y. Bian, Y. Su, J. Liu, and L. Zhu, "Dual-wavelength passively Q-switched erbium doped fiber laser based on an SWNT saturable absorber," Opt. Commun. **294**, 267–270 (2013).
17. Y. Huang, Z. Luo, Y. Li, M. Zhong, B. Xu, K. Che, H. Xu, Z. Cai, J. Peng, and J. Weng, "Widely-tunable, passively Q-switched erbium-doped fiber laser with few-layer MoS2 saturable absorber," Opt. Express **22**(21), 25258–25266 (2014).
18. Z. Yu, Y. Song, J. Tian, Z. Dou, H. Guoyu, K. Li, H. Li, and X. Zhang, "High-repetition-rate Q-switched fiber laser with high quality topological insulator Bi_2Se_3 film," Opt. Express **22**(10), 11508–11515 (2014).
19. E. I. Ismail, N. A. Kadir, A. A. Latiff, H. Ahmad, and S. W. Harun, "Black phosphorus crystal as a saturable absorber for both Q-switched and mode-locked erbium-doped fiber laser," RSC Advances **6**(76), 72692–72697 (2016).
20. N. N. Razak, A. A. Latiff, Z. Zakaria, and S. W. Harun, "Q-switched Erbium-doped Fiber Laser with a Black Phosphorus Saturable Absorber," Photonics Lett. Pol. **9**(2), 72–74 (2017).
21. B. Cole and L. Goldberg, "Highly efficient passively Q-switched Tm:YAP laser using a Cr:ZnS saturable absorber," Opt. Lett. **42**(12), 2259–2262 (2017).
22. M. Nematollahi, X. Yang, L. M. Aas, Z. Ghadyani, M. Kildemo, U. Gibson, and T. W. Reenas, "Molecular beam and pulsed laser deposition of ZnS:Cr for intermediate band solar cells," Sol. Energy Mater. Sol. Cells **141**, 322–330 (2015).
23. J. Dong, K. I. Ueda, H. Yagi, and A. Kaminskii, "Laser-diode pumped self-Q-switched microchip lasers," Opt. Rev. **15**(2), 57–74 (2008).
24. J. E. Williams, V. V. Fedorov, D. V. Martyshkin, I. S. Moskalev, R. P. Camata, and S. B. Mirov, "Mid-IR laser oscillation in Cr2+:ZnSe planar waveguide," Opt. Express **18**(25), 25999–26006 (2010).
25. C. Grivas, "Optically pumped planar waveguide lasers, Part 1: Fundamentals and fabrication techniques," Prog. Quantum Electron. **35**(6), 159–240 (2011).
26. B. L. Vanmil, A. J. Ptak, L. Boi, L. J. Wang, M. Chirila, N. C. Giles, T. H. Myers, and L. Wang, "Heavy Cr doping of ZnSe by molecular beam epitaxy," J. Electron. Mater. **31**(7), 770–775 (2002).
27. M. Luo, B. L. Vanmil, R. P. Tompkins, I. Cui, T. Mounts, U. N. Roy, A. Burger, T. H. Myers, and N. C. Giles, "Luminescence study of ZnTe:Cr epilayers grown by molecular-beam epitaxy," J. Electron. Mater. **32**(7), 737–744 (2003).
28. A. Gallian, V. V. Fedorov, J. Kernal, J. Allman, S. B. Mirov, E. M. Dianov, A. O. Zabezhaylov, and I. P. Kazakov, "Spectroscopic studies of molecular-beam epitaxially grown Cr2+-doped ZnSe thin films," Appl. Phys. Lett. **86**(9), 091105 (2005).
29. R. A. McFarlane, M. Lui, and D. Yap, "Rare earth doped fluoride waveguides fabricated using molecular beam epitaxy," IEEE J. Sel. Top. Quantum Electron. **1**(1), 82–91 (1995).
30. L. E. Bausa, R. Legros, and A. Muñoz-Yagüe, "Nd^{3+} incorporation in CaF_2 layers grown by molecular beam epitaxy," Appl. Phys. Lett. **59**(2), 152–154 (1991).
31. E. Daran, R. Legros, A. Muñoz-Yagüe, C. Fontaine, and L. E. Bausa, "1.54 μm wavelength emission of highly Er-doped CaF_2 layers grown by molecular beam epitaxy," J. Appl. Phys. **76**(1), 270–273 (1994).
32. X. Zhang, F. Lahoz, C. Serrano, G. Lacoste, and E. Daran, "1.3 μm emission of Nd:LaF_3 thin films grown by molecular beam epitaxy," IEEE J. Quantum Electron. **36**(2), 243–247 (2000).
33. E. Daran, D. P. Shepherd, T. Bhutta, and C. Serrano, "Laser operation of Nd:LaF_3 thin film grown by molecular beam epitaxy," Electron. Lett. **35**(5), 398–400 (1999).
34. T. Bhutta, A. M. Chardon, D. Shepherd, E. Daran, C. Serrano, and A. Muñoz-Yagüe, "Low phonon energy Nd:LaF_3 channel waveguide lasers fabricated by molecular beam epitaxy," IEEE J. Quantum Electron. **37**(11), 1469–1477 (2001).
35. R. A. Betts and C. W. Pitt, "Growth of thin-film lithium niobite by molecular beam epitaxy," Electron. Lett. **21**(21), 960–962 (1985).
36. R. A. McKee, F. J. Walker, J. R. Conner, E. D. Specht, and D. E. Zelmon, "Molecular beam epitaxy growth of epitaxial barium silicide, barium oxide, and barium titanate on silicon," Appl. Phys. Lett. **59**(7), 782–784 (1991).
37. E. A. Karhu, C. Ildstad, S. Poggio, V. Furtula, N. Tolstik, I. T. Sorokina, J. Belbruno, and U. Gibson, "Vapor deposited Cr-doped ZnS thin films: towards optically pumped mid-infrared waveguide lasers," Opt. Mater. Express **6**(9), 2947–2955 (2016).

Optical Materials EXPRESS

38. R. Swanepoel, "Determination of the thickness and optical-constants of amorphous-silicon," J. Phys. E Sci. Instrum. **16**(12), 1214–1222 (1983).
39. D. Minkov and R. Swanepoel, "Computerization of the optical characterization of a thin dielectric film," Opt. Eng. **32**(12), 3333–3337 (1993).
40. B. F. Aull and H. P. Jenssen, "Vibronic interactions in Nd:YAG resulting in nonreciprocity of absorption and stimulated emission cross sections," IEEE J. Quantum Electron. **18**(5), 925–930 (1982).
41. I. T. Sorokina, "Crystalline Mid-Infrared Lasers," in *Solid-State Mid-Infrared Laser Sources (Topics in applied physics, v. 89)*, I. T. Sorokina and K. Vodopyanov, eds. (Springer Berlin / Heidelberg, 2003).
42. A. Burger, K. Chattopadhyay, J. O. Ndap, X. Ma, S. H. Morgan, C. I. Rablau, C. H. Su, S. Feth, R. H. Page, K. I. Schaffers, and S. A. Payne, "Preparation conditions of chromium doped ZnSe and their infrared luminescence properties," J. Cryst. Growth **225**(2–4), 249–256 (2001).
43. F. Y. Lo, Y. C. Ting, K. C. Chou, T. C. Hsieh, C. W. Ye, Y. Y. Hsu, M. Y. Chern, and H. L. Liu, "Paramagnetic dysprosium-doped zinc oxide thin films grown by pulsed-laser deposition," J. Appl. Phys. **117**(21), 213911 (2015).
44. W. G. Nilsen, "Raman Spectrum of Cubic ZnS," Phys. Rev. **182**(3), 838–850 (1969).
45. Y. C. Cheng, C. Q. Jin, F. Gao, X. L. Wu, W. Zhong, S. H. Li, and P. K. Chu, "Raman scattering study of zinc blende and wurtzite ZnS," J. Appl. Phys. **106**(12), 123505 (2009).
46. J. E. Williams, D. V. Martyshkin, V. V. Fedorov, I. S. Moskalev, R. P. Camata, and S. B. Mirov, "Cr:ZnSe planar waveguide mid-IR laser," Proc. SPIE **7912**, 79121H (2011).
47. S. H. Su, M. Yokoyama, and Y. K. Su, "Reactive ion etching of ZnS films using a gas mixture of methane/hydrogen/argon," Jpn. J. Appl. Phys. **37**(1), 1764–1767 (1998).
48. T. Yokogawa, M. Ogura, and T. Kajiwara, "Low-loss short-wavelength optical waveguides using ZnSe-ZnS strained-layer superlattices," Appl. Phys. Lett. **52**(2), 120–122 (1988).
49. Y. P. Peng, X. Zou, Z. Bai, Y. Leng, B. Jiang, X. Jiang, and L. Zhang, "Mid-infrared laser emission from Cr:ZnS channel waveguide fabricated by femtosecond laser helical writing," Sci. Rep. **5**(1), 18365 (2016).
50. A. Okhrimchuk, M. Smayev, V. Likhov, E. Sorokin, N. Tolstik, and I. T. Sorokina, "Femtosecond laser writing of the depressed cladding buried channel waveguides in ZnS crystal," Approved for publication in High-brightness Sources and Light-driven Interactions Congress 2018 (EUV&XRAY, HILAS, MICS), OSA Technical Digest (online) (Optical Society of America, 2018).
51. G. Renz, J. Speiser, A. Giesen, I. T. Sorokina, and E. Sorokin, "Cr:ZnSe thin disk cw laser," Proc. SPIE **8599**, 85991M (2013).
52. N. A. Tolstik, S. V. Kurilchik, V. E. Kisel, N. V. Kuleshov, O. V. Pilipenko, E. V. Koporulina, and N. I. Leonyuk, "Efficient diode-pumped Er,Yb:YAB laser," presented at XII Conference on Laser Optics (LO-2006), St.Petersburg, Russia, 26–30 June 2006, paper TuR1–05.
53. N. A. Tolstik, S. V. Kurilchik, V. E. Kisel, N. V. Kuleshov, V. V. Maltsev, O. V. Pilipenko, E. V. Koporulina, and N. I. Leonyuk, Spectroscopy and efficient laser operation of Er,Yb:$YAl_3(BO_3)_4$ crystal, in Proceedings of 2nd EPS-QEOD Europhoton Conference on Solid-State and Fiber Coherent Light Sources, Pisa, Italy, 10–15 September 2006, paper TuC13.
54. N. A. Tolstik, S. V. Kurilchik, V. E. Kisel, N. V. Kuleshov, V. V. Maltsev, O. V. Pilipenko, E. V. Koporulina, and N. I. Leonyuk, "Efficient 1 W continuous-wave diode-pumped Er,Yb:$YAl_3(BO_3)_4$ laser," Opt. Lett. **32**(22), 3233–3235 (2007).
55. N. A. Tolstik, V. E. Kisel, N. V. Kuleshov, V. V. Maltsev, and N. I. Leonyuk, "Er,Yb:$YAl_3(BO_3)_4$ – efficient 1.5 μm laser crystal," Appl. Phys. B **97**(2), 357–362 (2009).
56. V. V. Maltsev, E. V. Koporulina, N. I. Leonyuk, K. N. Gorbachenya, V. E. Kisel, A. S. Yasukevich, and N. V. Kuleshov, "Crystal growth of CW diode-pumped (Er^{3+},Yb^{3+}):$GdAl_3(BO_3)_4$ laser material," J. Cryst. Growth **401**, 807–812 (2014).
57. K. N. Gorbachenya, V. E. Kisel, A. S. Yasukevich, V. V. Maltsev, N. I. Leonyuk, and N. V. Kuleshov, "Highly efficient continuous-wave diode-pumped Er, Yb:$GdAl_3(BO_3)_4$ laser," Opt. Lett. **38**(14), 2446–2448 (2013).
58. K. N. Gorbachenya, V. E. Kisel, A. S. Yasukevich, V. V. Maltsev, N. I. Leonyuk, and N. V. Kuleshov, "Eye-safe 1.55 μm passively Q-switched Er,Yb:$GdAl_3(BO_3)_4$ diode-pumped laser," Opt. Lett. **41**(5), 918–921 (2016).

1. Introduction

Transition metal doped zinc chalcogenides are of interest as nonlinear optical materials in the mid infrared, both as active media and saturable absorbers. Continuous-wave (CW) and ultrashort-pulsed sources based on Cr^{2+}-doped II-VI crystals [1–8] have come of age and are entering the real-world applications [3,8]. In particular, Cr^{2+}:ZnS-based laser systems exhibit robustness, mechanical and optical stability, tens of Watts average power, ultra-broad tuning between 1.9 and 3.2 μm in continuous-wave regime, tens of nJ and GHz repetition rate in femtosecond pulsed regime [3,6], more than 1.5 octave supercontinuum extending from 1.2 to 3.6 μm [9] and direct diode-pumping [10].

Transition metal doped zinc chalcogenide bulk crystals are also known as efficient saturable absorbers for Q-switching in the spectral range 1.5-1.6 μm [11,12]. Co^{2+} ion is

Optical Materials EXPRESS

commonly used as a dopant for absorbers for 1.5-1.6 μm erbium lasers, with Cr^{2+} being a main choice for 1.9-2.0 μm thulium lasers. The advantages of saturable absorbers based on Cr^{2+}-doped crystals are high ground-state absorption cross-sections (~10^{-19} cm^2) and negligible excited-state absorption losses [12]. Recently, 1.5-1.6 μm passively Q-switched operation has been demonstrated using a number of different novel 2-D materials like single-walled carbon nanotubes, graphene, topological insulators, transition-metal di-chalcogenides and black phosphorus [13–20]. However, these experiments resulted in rather low laser pulse energies typically not exceeding ~1 μJ. Much higher pulse energy of 0.6 mJ was extracted from Tm:YAP laser Q-switched by crystalline Cr:ZnS saturable absorber [21], thus making it a proper choice for the high-energy laser systems.

The real-world applications of Cr:ZnS lasers would strongly benefit if these lasers could be produced in a simple and robust waveguide form. The first steps in compact laser fabrication have been made, using inscription of a waveguide structure in a bulk crystal [7] and thin films fabrication has been reported [22], although the pulsed laser deposition (PLD) in that study did not provide the desired optical quality. For Q-switched lasers, a microchip configuration [23] is advantageous due to its robustness, adjustment simplicity, and potential for short pulse generation. Realization of a true monolithic microchip with integrated saturable absorber requires advanced technological solutions. One approach is the growth of crystalline thin films of saturable absorber directly on the active laser medium, with structural quality good enough to permit subsequent deposition of a dielectric mirror. The first steps have also been made here with a demonstration of PLD-grown Cr:ZnSe thin films acting as a saturable absorber for Er:YAG laser [24].

The reliable and capable technique of molecular beam epitaxy/ultra/high vacuum (MBE/UHV) offers technological advantages over PLD. MBE is widely used for the fabrication of semiconductor devices, and allows deposition of ultra-high purity layers with accurate control of composition and thickness of the films [25], as well as rapid turnaround for variations of the parameters. Transition-metal-doped MBE-grown thin films of ZnSe were reported about a decade ago [26–28], but with very limited spectroscopic characterization. Reports on the epitaxial growth of the rare-earth-doped active optical waveguides are limited to fluorides [29–34] and few oxide materials [35,36]. Laser action was so far demonstrated only in MBE-grown Nd^{3+}:LaF_3 structures with slab and channel geometries [33,34]. It is important to point out that the combination of low growth temperatures used here, and inherently low growth rates of the MBE method ensures homogeneous distribution of the rare-earth ions within the layers and thus minimization of clustering [25]. Particularly for fluorides it allowed significantly higher dopant ion concentrations in MBE-grown films compared to the corresponding bulk crystals [31]. Among the limitations of the method one can mention high equipment cost, limited flexibility in terms of using the same equipment for depositing a range of different materials (purity issues), and typically low deposition rates (not exceeding ~0.7 μm/h for fluorides [33]).

Recently we reported the deposition of the first MBE/UHV-grown Cr:ZnS films [37]. This article extends the work with a comparative study of the spectral-luminescent properties of thin films and bulk crystals, demonstrating the readiness of this technology for laser applications. We also demonstrate the first use of these films for Q-switching.

2. Material fabrication

The main purpose of the study was to investigate the Cr:ZnS films grown by the high vacuum (MBE/UHV method), where the deposition parameters can be controlled within tight tolerances. Deposition rates were constant within 5%, substrate temperature increased less than a few degrees due to the larger separation between the sources and substrate, and H_2O contamination was minimal. A comparison was made to films deposited in a conventional diffusion-pumped vacuum system to see if comparable fluorescence could be obtained with a lower-cost, more scalable deposition technique.

Optical Materials EXPRESS

For the thin films of Cr:doped ZnS in the ultra-high vacuum MBE system we used high purity (99.999%) materials, deposited at a base pressure of $6 \cdot 10^{-7}$ Pa. Substrates used included: single crystalline silicon with (100) orientation, single crystalline silicon with a 1 μm SiO_2 coating, CaF_2, and, for optical characterization, c-plane sapphire. The films were deposited on either unheated (RT) substrates or on substrates heated up to 200 °C; several RT-deposited films were subsequently annealed at 400 °C for 12 hours. Energy dispersive X-ray spectroscopy (EDX) performed in a Hitachi TM3000 electron microscope was used to determine the concentration in calibration films with high Cr content. For lower concentrations, the composition was estimated from the rations of the deposition rates [37]. The film thicknesses were measured using a stylus profilometer (Tencor Alphastep).

Films were grown with Cr concentrations ranging from $1.3 \cdot 10^{18}$ to $3.4 \cdot 10^{20}$ cm^{-3} (1 at. % gives $1.27 \cdot 10^{20}$ cm^{-3}) and thicknesses from 2 to 12 μm. The maximum thickness of the films was limited by the volume of the Knudsen cells in the MBE setup. Films were found to be polycrystalline (typical lateral grain size about 30 nm) with high transparency through the visible and infrared regions. Films deposited at 200 °C showed a transmission rolloff in the wavelength region below 1.4 μm, most probably due to scattering caused by increased surface roughness and crystallite size. Films with Cr concentrations greater than $6 \cdot 10^{19}$ cm^{-3} also had excess short wavelength absorption. The crystalline structure was a mix of the hexagonal wurtzite and cubic sphalerite forms of ZnS, and Cr doping appeared to favor the cubic structure. More details on deposition technique and structural characterization of the films can be found in a separate article [37].

We also deposited several films in a diffusion pumped chamber, using 99.99% pure ZnS and Cr-plated W rods (R.D. Mathis) as sources. This system had a base pressure of ~$2 \cdot 10^{-6}$ Pa, with pressures rising to $2 \cdot 10^{-5}$ Pa during deposition. Using a Luxel Radak source, ZnS deposition rates were more than a factor of two higher than for the MBE/UHV films. Using a reduced distance between the source and the substrate, the film thickness was increased to 25 μm.

3. Spectroscopic characterization and potential as laser active media

Different spectroscopic techniques were used to characterize optically active divalent chromium ions. In particular the absorption, fluorescence, and Raman spectra were measured, and fluorescence kinetics were recorded and analyzed.

3.1 Absorption and emission spectroscopy

The absorption spectra were measured within the spectral range 600-2500 nm using an OLIS UV-VIS_IR spectrophotometer. A well-defined absorption band centered at 1.7 μm relates to the $^5T_2 \rightarrow {}^5E$ transition of Cr^{2+} ion (Fig. 1). Thin film interference effects were readily observable in thin Cr:ZnS films in the transmission spectra (Fig. 1(a)). Swanepoel analysis [38,39] was applied to filter out these oscillations and derive the refractive index and absorption coefficient, α. Some spectral distortions remained visible around 800 nm (Fig. 1(b)), where the detector on the spectrometer changes. Some background losses in the absorption spectra of the films are caused by the Rayleigh scattering on the small Cr:ZnS crystallites formed during the film deposition [37]. These losses tend to increase for films with higher dopant concentration (Fig. 1(b)), but are also strongly influenced by the deposition conditions (temperature, annealing, etc.). Unheated substrates (with resulting small lateral grain size) led to reduced scatter and absorption. The absorption spectrum of Cr(0.04 at.%):ZnS single crystal (Fig. 1(c)) is almost free of those losses.

Optical Materials EXPRESS

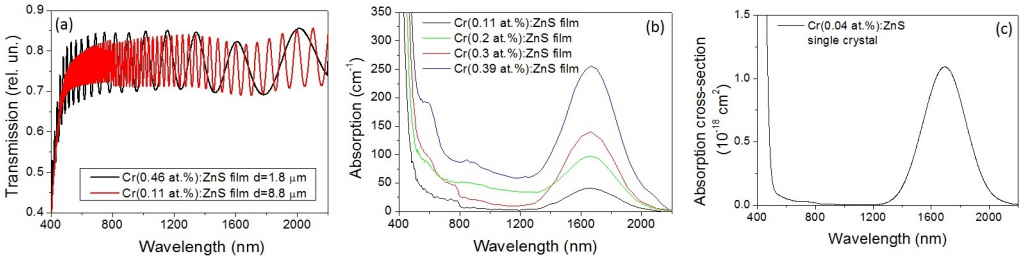

Fig. 1. The raw transmission data (a) and the absorption spectra (b) of series of MBE-grown Cr:ZnS thin films with different dopant concentrations (data processed by Swanepoel analysis [38,39]), and absorption cross-section spectrum of Cr:ZnS single crystal (c).

The fluorescence spectra of Cr:ZnS films were excited by 1.55-μm erbium fiber laser and detected using a commercial FTIR spectrometer (Nicolet Nexus 870). The emission band around 2.0 μm relates to $^5E \rightarrow {}^5T_2$transition of Cr^{2+} ion. Fluorescence spectra of three different samples are shown in Fig. 2(a), and intensity modulations are the result of the interference effect mentioned above. The spectra are normalized, and it is important to note that the film with doubled Cr^{2+} concentration provides 5x lower fluorescence signal under the same experimental conditions, giving evidence of concentration quenching. The emission cross-section spectra were calculated according to the Füchtbauer-Ladenburg equation [40]. The radiative lifetime required for the calculation (6.7 μs) was measured at 77K for the Cr:ZnS single crystal with a 0.015 at% Cr doping level, as the signal from thin film samples was too noisy for accurate low-temperature lifetime measurements (Fig. 3). It is shown below that the measured room-temperature fluorescence lifetimes of thin film samples are very close to those of single crystals with similar concentrations, so we assume that the low-temperature lifetimes are comparable as well. The comparison of the spectra for Cr:ZnS single crystal and 4.6-μm thick film with $C_{cr} = 3.8 \cdot 10^{18}$ cm^{-3} is given in Fig. 2(b). Aside from the modulation in the film spectrum due to interference, the spectra look very similar.

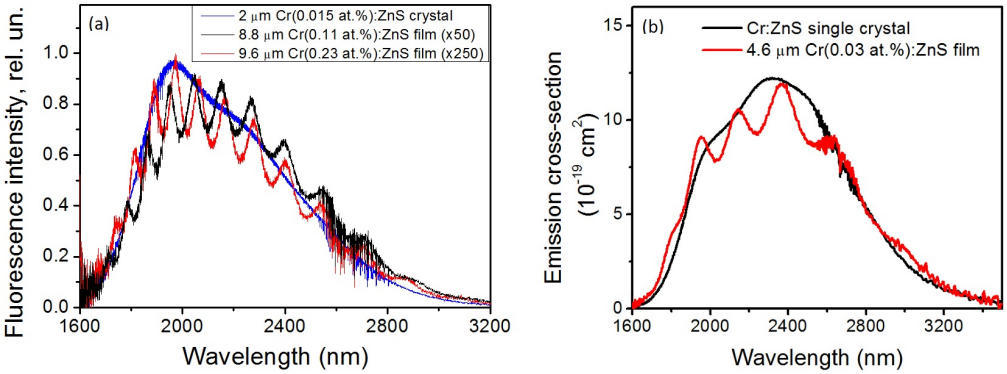

Fig. 2. The fluorescence spectra (a), and the emission cross-sections (b) of the Cr:ZnS thin films and single crystal

3.2 Fluorescence kinetics and concentration quenching

Temperature and concentration quenching of Cr^{2+} fluorescence in chalcogenides is a well-known effect [41,42], and 2-μm fluorescence is quenched in ZnS crystal at room temperature. In this paper, the dependence of fluorescence quenching on active dopant concentration was investigated, in terms of both lifetime and relative efficiency.

Fluorescence lifetimes of thin Cr:ZnS films were measured using emission of a current-modulated laser diode at 1630 nm and a 77 K-cooled InSb photodetector with response time around 0.3 μs. Fluorescence kinetics are shown in Fig. 3(a). Because the samples are very

Optical Materials EXPRESS

thin, the pump absorption is quite small, especially for the low-concentration samples, and the overall signal level is very low. This explains the high noise level on the curves, despite the long averaging time. The fluorescence decay curve of a sample with the lowest available Cr concentration of $1.3 \cdot 10^{18}$ cm^{-3} (red curve in Fig. 3(a)) was found to be single-exponential with a lifetime of about 5.4 μs, which is very close to the Cr^{2+} lifetime in the Cr:ZnS single crystal with similar concentration (black curve on Fig. 3(a)). An increase of the Cr^{2+} concentration in the films results in a shortening of the measured lifetime due to the concentration quenching effect. For the active ion concentration of $1.4 \cdot 10^{19}$ cm^{-3} the measured lifetime dropped down to 1.1 μs (dark yellow curve in Fig. 3(a)). Further increase of Cr^{2+} concentration brings the measured lifetime value to the range of the photodetector response time (~0.3 μs).

The alternative way to characterize the fluorescence quenching is through the dependence of integrated fluorescence intensity on active ion concentration using continuous-wave excitation. The experimental conditions were held constant through the whole measurement series. A sensitive thermoelectrically-cooled amplified InGaAs photodetector with a 3 mm photosensitive area diameter (Hamamatsu G5853-23) was used for these measurements. The emission of an Er:fiber laser at 1.61 μm wavelength used as the excitation source, was coupled into a single-mode optical fiber and positioned very close to the to the surface of the film under characterization, thus ensuring proper positioning and high intensity of the excitation beam. The fluorescence signal was collected on an input slit of a 1/8 m compact monochromator (Spectral Products CM110) using a CaF_2 focusing lens. The signal from the photodetector that was installed on the output slit of the monochromator, was measured using a lock-in amplifier, and normalized to the absorbed excitation power calculated using the Cr^{2+}absorption coefficient and the layer thickness. These measurements did not require the spectrometer to be calibrated using a black-body radiation source. The high sensitivity of the setup allowed an expansion of the concentration range of measured samples up to $5 \cdot 10^{19}$ cm^{-3}. The measurements results (Fig. 3(b)) show concentration quenching of the normalized fluorescence signal down to 0.5% of its maximal value. The reference measurement was performed with the 2.5-mm-thick Cr:ZnS single crystal with concentration of $2 \cdot 10^{18}$ cm^{-3} (red point on the Fig. 3(b)). Results show that the relative fluorescence efficiencies of the grown films are equal to those of Cr:ZnS single crystal, giving evidence of the high material quality and potential suitability for laser experiments.

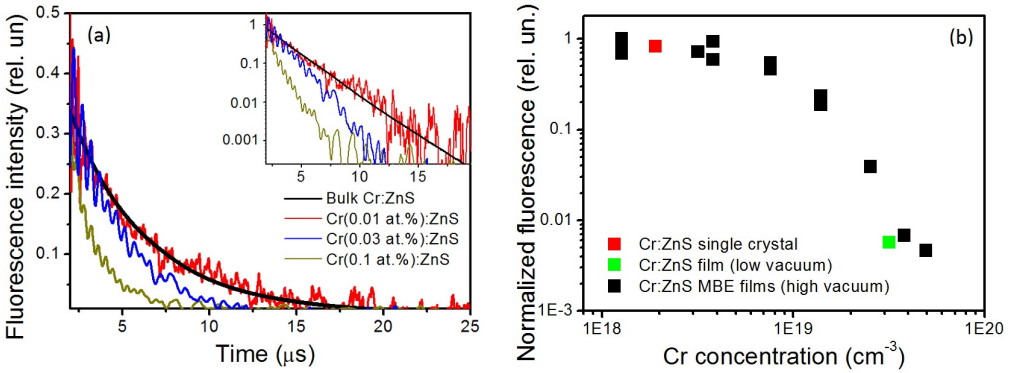

Fig. 3. The fluorescence kinetics of the low-concentrated Cr:ZnS film samples at room temperature (a), the dependence of the fluorescence relative intensity (normalized quantum yield) on Cr^{2+} concentration (b).

It is important also to point out that the film deposited in the diffusion-pumped system, where the deposition rate control was less precise than in the ultra-high vacuum system, fluoresced with comparable efficiency to UHV films with similar Cr concentrations (green

Optical Materials EXPRESS

point on the Fig. 3 (b)). This demonstrates that the fluorescence is tolerant of a wide range of thermal deposition methods, and that low-cost, fast turnaround systems can be employed.

3.3 Raman spectroscopy

Raman spectra were measured using a Renishaw InVia Reflex spectrometer with circularly polarized 532 nm laser excitation. Figure 4 shows 1st and 2nd order Raman spectra of the bulk ZnS crystal and MBE-grown Cr:ZnS thin films with different concentrations on top of the sapphire substrate. The substrate spectrum shows Al_2O_3 peaks at 379 cm^{-1} and 577 cm^{-1} [43], which are also present in all the thin film spectra. Bulk crystalline ZnS exhibits a number of maxima, particularly in the 200-350 cm^{-1} and 600-700 cm^{-1} ranges, typical for both cubic and wurtzite ZnS [44,45]. The appearance of a side lobe at 698 cm^{-1} and a narrow peak at 275 cm^{-1}confirms the presence of some ZnS wurtzite phase [45]. Spectra of undoped and $3.8 \cdot 10^{18}$ cm^{-3} doped films are similar to those of a ZnS single crystal, but with broadening of the lines probably caused by the slightly disordered structure of the films. For the films doped with $1.3 \cdot 10^{19}$ cm^{-3} of Cr^{2+} the 2nd order Raman peaks of ZnS seem to be less pronounced, and additional side lobe of the Cr:ZnS LO peak at 325 cm^{-1} [44] is observed. At higher Cr concentrations, further distortions of the Raman spectra appear; evidence of a highly disordered structure which is different from cubic and hexagonal ZnS. It is worth noting that the targeted doping level for Cr:ZnS films for laser applications is below $1.3 \cdot 10^{19}$ cm^{-3}, and no distortions of Raman spectra are observed in that range.

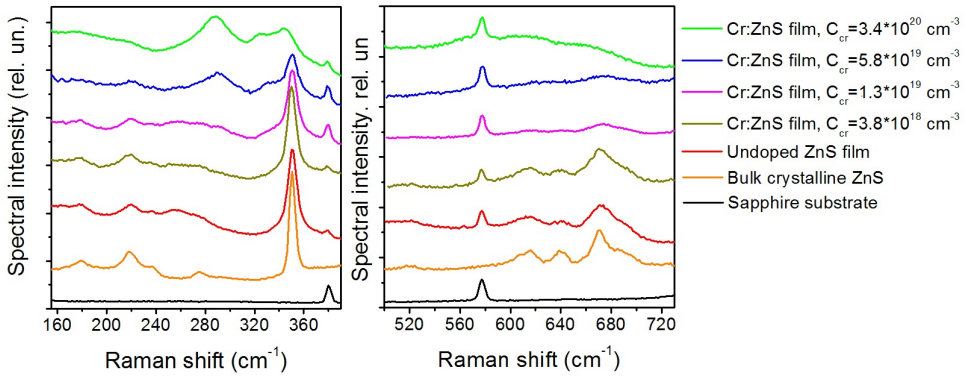

Fig. 4. Raman spectra of the sapphire substrate (black line), Cr:ZnS single crystal (orange line), and Cr:ZnS MBE-grown films with different Cr concentrations.

3.4 Potential as a laser medium

Since the refractive index of Cr:ZnS at 2.4 μm (2.26) is higher than that of sapphire (1.73), the manufactured sapphire/Cr:ZnS/air structure should provide planar waveguiding. Since the refraction index difference is rather large, multimode waveguiding is assumed. The propagation losses of the waveguide were measured to be around 8 dB/cm at 1 μm wavelength [37], and we expect much lower value at 2.4 μm due to weaker Rayleigh scattering. Still rather high losses are expected on the input/output facets of the as-grown waveguide, since no measures could be taken to ensure the optical quality of the interface during growth, and mechanical processing (cutting/polishing) of the facets for such a structure is challenging due to considerably different physical properties of the materials involved. For these reasons laser emission in PLD-grown Cr:ZnSe films was only demonstrated using a high-peak-power pulsed nanosecond pump source, but laser experiments were unsuccessful for CW pumping [46]. Similarly, our experiments to demonstrate the planar waveguide lasing in as-grown Cr:ZnS crystalline thin film by pumping with a CW erbium fiber laser at 1.61 μm were not successful. Proper processing of the facets

Optical Materials EXPRESS

and structuring of the films to form a channel waveguide is a key to success on this way. Reactive ion etching [47], ridge waveguide formation by photolithography [48], or femtosecond laser writing [7,49] could be implemented to further improve the waveguiding for both the pump and the laser beam thus increasing the pump intensity and reducing the threshold. We have made preliminary experiments with femtosecond laser writing in bulk crystalline ZnS [50] and are moving forward towards using this technology for thin film samples.

As an alternative approach, thin films of Cr:ZnS grown on a substrate with large thermal conductivity have high potential for the thin disk laser technology. Thin-disk Cr:ZnSe laser have been successfully demonstrated [51] providing up to 5 W output power for 250-μm-thick active crystal. The thickness of vapor-deposited films demonstrated in this work was limited by volume of the material source to 25 μm. Implementation of the material source with higher volume in the deposition chamber would allow us to grow the films thick enough to be used in thin disk laser, with an advantage of considerably higher thermal conductivity of Cr:ZnS in comparison with Cr:ZnSe.

4. Cr:ZnS thin films as saturable absorbers

The Q-switching performance of the films was tested in the microchip configuration, where the physical dimensions of the elements are critical. A dip-seeded solution grown Er(1.0 at.%),Yb(11 at.%):$GdAl_3(BO_3)_4$ (GdAB) crystal was used as the gain element of the laser. This material belongs to a family of erbium-ytterbium co-doped borate crystals [52,53] which are known for scaling the average power of 980-nm-pumped erbium lasers emitting around 1.55 μm beyond 1 W [54,55]. Crystal growth, spectroscopy, CW and Q-switched laser action with Er,Yb:GdAB have been reported recently [13,14,56–58] showing a great potential of the material for the development of compact eye-safe lasers for real-life applications.

The Q-switched laser experiments were performed in the compact microchip cavity (Fig. 5(a)). The cavity consisted of pump mirror (PM) (R>99.5% at 1522 nm and T>95% at 976 nm) deposited onto external side of the active crystal and a flat output coupler (OC). The active element (AE), a 1mm-thick, c–cut Er,Yb:GdAB crystal, was wrapped in indium foil and mounted between two TE-cooled copper slabs with a hole in the center to permit transmission of the pump and laser beams. The saturable absorber (SA) Cr:ZnS crystalline layer was deposited onto 1 mm-thick sapphire substrate and inserted between the active element and OC. We tested two different Cr(0.11 at%):ZnS films as saturable absorbers, with thicknesses of 1.8 μm and 8.8 μm, corresponding to initial transmissions of 99.5% and 98.5% at the laser wavelength (T_0). An OC with rather high transmission of 9% at laser wavelength was used in order to reduce the intracavity energy density and prevent damage of the saturable absorber (SA). An 8 W, 976 nm unpolarized fiber-coupled (Ø105 μm, NA = 0.22) laser diode was used as a pump source. The pump beam was focused into 120 μm spot ($1/e^2$ intensity) inside the crystal. The minimal possible geometrical cavity length was limited to 4 mm by the design of the active element cooling system.

Stable passively Q-switched operation of the Er,Yb:GdAB laser with Cr:ZnS thin film saturable absorber was obtained. Using an SA with a T_0 = 99.5%, laser pulses with an energy of 5.7 μJ and duration of 22 ns were obtained at a 1522 nm. The maximal repetition rate was as high as 130 kHz when the incident pump power was 6.5 W. The highest pulse energy of 9.2 μJ and the shortest pulse duration of 8 ns were obtained when SA with a T_0 = 98.5% was used. The repetition rate did not exceed 42 kHz in this case (Fig. 5 (b)). The oscilloscope trace of the shortest single Q-switched pulse measured with corresponding pulse train is shown in Fig. 5(c). The output beam had a close to TEM_{00} spatial profile with M^2 parameter less than 1.5.

Optical Materials EXPRESS

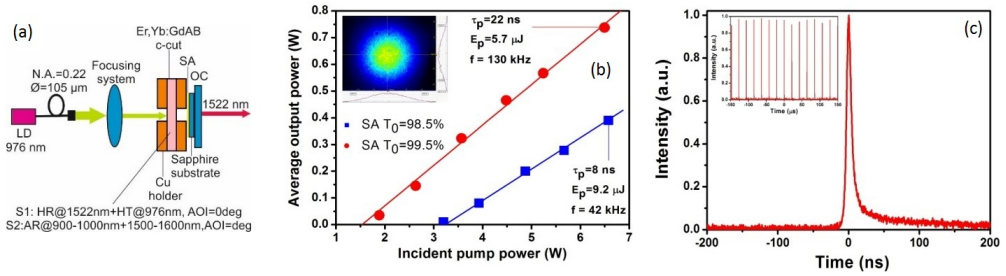

Fig. 5. The experimental setup for Q-switched laser experiments with Cr:ZnS thin film saturable absorber (a), input-output characteristics of Er,Yb:GAB laser Q-switched by Cr:ZnS saturable absorber (inset shows the beam profile) (b), oscilloscope trace of the shortest optical pulse obtained from Cr:ZnS Q-switched Er,Yb:GAB laser (inset shows the corresponding pulse train) (c).

It is worth noting that Cr:ZnS saturable absorbers used in these experiments were not antireflection-coated and thus acted as intracavity etalons. It resulted in additional cavity losses reducing overall performance of the system. Although in the current experiment the saturable absorber was implemented as a separate optical element, we point out that MBE/UHV deposition of the Cr:ZnS saturable absorber film directly onto the active crystal would demonstrate an approach to a fully integrated monolithic microchip laser. Such direct deposition is feasible for various active media as confirmed by deposition experiments with oxides, fluorides and silicon.

5. Conclusion

The extensive comparative analysis of the MBE-grown Cr:ZnS thin films and Bridgman grown Cr:ZnS single crystals with Cr^{2+} concentrations below $1 \cdot 10^{19}$ cm^{-3} show structural and spectral-luminescent properties of thin films to be similar to those of Cr:ZnS single crystals. Concentration quenching effects play an important role in films with higher Cr^{2+} content, leading to a dramatic decrease of the fluorescence efficiency and further structural disorder. Cr:ZnS films were successfully implemented as saturable absorbers for an Er,Yb:GdAB Q-switched solid-state laser. Vapor deposition, even without ultrahigh vacuum, can be used to synthesize laser-quality Cr:ZnS films with thickness up to 25 μm, usable as active and passive elements of solid-state lasers, particularly thin-disk and waveguide lasers emitting in the mid-IR spectral range.

Funding

NFR NANO 2021 (219686); FWF (P24916); ATLA Lasers AS.